THE JOURNAL OF PHYSICAL CHEMISTRY B

Article

Cite This: J. Phys. Chem. B 2017, 121, 10417-10428

pubs.acs.org/JPCB

Discontinuity in Fast Dynamics at the Glass Transition of *ortho*-Terphenyl

David J. Hoffman and Michael D. Fayer*

Department of Chemistry, Stanford University, Stanford, California 94305, United States

ABSTRACT: The dynamics of the molecular glass former *ortho*-terphenyl through the glass transition were observed with two-dimensional infrared vibrational spectroscopy measurements of spectral diffusion using the small probe molecule phenylselenocyanate. Although the slow diffusive motions were not visible on the experimental time scale, a picosecond-scale exponential relaxation was observed at temperatures from above to well below the glass transition temperature. The characteristic time scale has a smooth temperature dependence from the liquid into the glass phase, but the range of vibrational frequencies the probe samples displayed a discontinuity at the glass transition temperature. Complementary pump-probe experiments associate the observed motion with density fluctuations. The key features of the dynamics are reproduced with a simple corrugated well potential energy surface model. In addition, the temperature dependence of the homogeneous vibrational dephasing was found to have a T^2 functional form, where T is the absolute temperature.

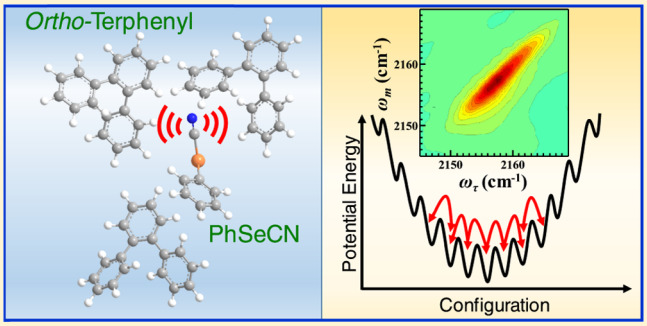

I. INTRODUCTION

The microscopic mechanism of how a liquid becomes a glass remains a difficult open question in condensed matter physics.[1−5] Besides the heavily studied, characteristically slow glassy dynamics, an ultrafast picosecond-scale process has also been observed in a wide range of glass formers with a variety of techniques. In *ortho*-terphenyl (OTP, structure in Figure 1), one of the best studied molecular glass formers, picosecond-scale dynamics have been observed in the glass phase with incoherent neutron scattering,[6] NMR,[7] depolarized light scattering,[8,9] Brillouin light scattering,[10] and photon correlation spectroscopy.[11] A similar feature is seen in a variety of molecular dynamics simulations of OTP,[12,13] generally manifesting as the fast part of the characteristic two-step relaxation at low temperatures.

The observed ultrafast process is frequently described in terms of mode coupling theory (MCT).[6−9,11,14] The "fast β" relaxation predicted by MCT is a universal feature in glass formers typically described as the motion of particles that are "caged" by their neighbors prior to longer time scale diffusive motions.[15,16] MCT has been very successful in describing many dynamical properties of mildly supercooled liquids but suffers notable breakdowns as the glass transition is approached. Experimental results in the glassy regime have sometimes matched the qualitative descriptions of extended MCT models,[8] but other models involving phonon fluctuations[17] or vibrational−translational coupling[18] have also been invoked.

To study the ultrafast processes in supercooled and glassy OTP, two-dimensional infrared (2D IR) vibrational echo spectroscopy was employed. 2D IR reports on the time evolution of structures in the system through the "spectral diffusion" experienced by vibrational probes on picosecond timescales.[19,20] As the sample structure evolves with time, the resonant frequency of the vibrational probe changes concurrently. The frequency evolution induced by structural evolution of the medium is referred to as spectral diffusion, which can be observed and quantified with 2D IR. The 2D IR data yields the frequency−frequency correlation function (FFCF) that gives the characteristic timescales of structural rearrangement of the sample as well as the range of frequencies sampled.

As most vibrational modes have lifetimes of only a few picoseconds in condensed phases, it is necessary to introduce long-lived vibrational probes to observe dynamics over many decades in time. Toward this end, the OTP sample was doped with 5 mol % of phenylselenocyanate (PhSeCN, structure in Figure 1). The CN stretches of molecular selenocyanates have lifetimes that are many hundreds of picoseconds[21] and have been used to study both complex liquid[22−24] and protein[25,26] dynamics. Further, it has been demonstrated that chemically similar, long-lived probes experience dynamics that are nearly identical to those experienced by molecules in the bulk liquid.[27] In addition, PhSeCN and another long-lived vibrational probe used to study the dynamics of deeply supercooled benzophenone with 2D IR as a function of temperature gave a single master curve.[24]

2D IR has been used previously to study both OTP and the similar liquid benzophenone in the liquid and supercooled liquid regimes.[24] The 2D IR experiments on the liquid phase of OTP revealed slow diffusive components that changed sharply

Received: August 19, 2017
Revised: October 12, 2017
Published: October 17, 2017

DOI: 10.1021/acs.jpcb.7b08301
J. Phys. Chem. B 2017, 121, 10417−10428

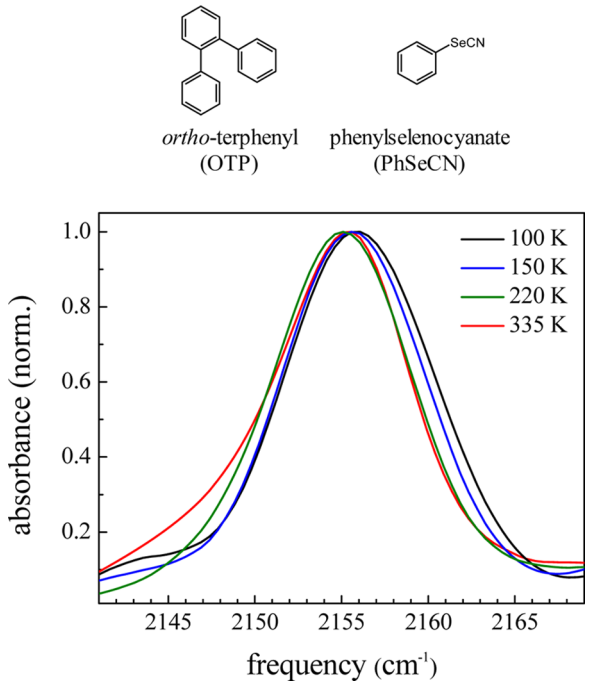

Figure 1. Top: Molecular structures of the glass former *ortho*-terphenyl (OTP) and vibrational probe phenylselenocyanate (PhSeCN). Bottom: Fourier transform infrared (FT-IR) spectra of the nitrile stretch of PhSeCN in OTP at a range of temperatures. The stretch slightly broadens and shifts to higher frequency deep in the glass phase.

with temperature, in agreement with other 2D IR studies on similar glass forming liquids.[28,29] In addition to these slow motions, a picosecond time scale relaxation that had very mild temperature dependence was seen. Although the slow motions at low temperature occur on timescales far slower than is measurable with vibrational probes because of the time span limitation set by the vibrational lifetime, the fast dynamics could still be well resolved at the lowest temperature studied.

This work expands the previous study to look at the fast dynamics in the glass phase of OTP. The fast process, which is a clear continuation of the process in the liquid, is visible in the glass until ∼180 K, which is approximately 60 K below the glass transition temperature. The Arrhenius temperature dependence previously found for the time scale of the fast process in the liquid continues smoothly into the glass phase. Similarly, the range of frequencies sampled by the probe during the fast process continues to decline with decreasing temperatures, as more of the possible spectral diffusion requires slow diffusive motions to occur. The temperature dependence of the range of frequencies sampled is found to have the exact opposite temperature dependence as the characteristic time scale, such that their product is temperature invariant.

Although the product of the characteristic time scale and the range of sampled frequencies is found to be temperature independent above and below the glass transition temperature, T_g, the product undergoes a step discontinuity at the glass transition, that is, the product is one temperature-independent constant in the liquid phase and a different temperature-independent constant in the glass phase. As the characteristic time scale varies smoothly with temperature through the glass transition, the discontinuity is in the range of sampled frequencies. This discontinuity is distinct from the temperature dependence of previously reported fast processes in OTP.

To better understand the physical origin of this fast process, companion polarization-selective pump-probe (PSPP) experiments were performed for a range of temperatures in the liquid and glass phase of OTP. PSPP experiments measure orientational relaxation of the vibrational probe molecule.[30] The experiments showed that in the glass phase, the probe reorientation is extremely slow, at least an order of magnitude slower than that of the fast spectral diffusion. This confirms that the fast spectral diffusion is not caused by fast, small-angle orientational fluctuations of the probe molecule and strongly suggests that small-angle orientational motions of the bulk liquid are not responsible either.

The asymptotic scaling laws from MCT and their applicability to the 2D IR data were also examined.[15,16] It was found that the low-temperature data does not appear to satisfy the power law decay predicted by MCT, despite having superficial similarity to the fast relaxation to a plateau predicted by the MCT equations. It is possible that a more complex formulation of schematic MCT correlators are needed to describe the data or that the motions responsible for spectral diffusion are unrelated to the fast β-process in MCT.

A simple numerical model of a random walk on a one-dimensional schematic potential energy surface was used to describe the key temperature-dependent thermodynamic characteristics of the fast spectral diffusion process. The free energy landscape was modeled as a single rough minimum,[1−4,31] with many small local minima spread across the one large potential well. Decreasing the temperature decreases the rate at which the local minima are sampled, as well as the range of wells sampled, reducing the frequency range while increasing the characteristic time scale of a calculated "frequency" autocorrelation function. For a range of temperatures, this model was found to reproduce the observed behavior of the spectral diffusion. Simple modifications to the potential were then employed to account for the discontinuity in the frequency amplitude at T_g.

II. EXPERIMENTAL SECTION

II.I. Sample Preparation. OTP was purchased from TCI America and purified by vacuum distillation before use. PhSeCN was purchased from Sigma-Aldrich and used without further preparation. A solution of 5 mol % PhSeCN in OTP was prepared for use in experiments. Previously performed differential scanning calorimetry experiments gave a melting point (T_m) of 328 K and a glass transition temperature (T_g) of 245 K for the PhSeCN in OTP solution.[24] The solution was heated above the OTP melting point to about 50 °C and loaded between two 3 mm CaF_2 windows separated by a 190 μm Teflon spacer. The windows were contained in a copper cell to make good thermal contact.

The cell was placed in a continuous-flow cryostat with CaF_2 windows. The temperature was controlled to well below 1 K by managing the flow of liquid nitrogen and the use of a PID heating element in the cryostat. For temperatures above 225 K, the OTP solution was cooled at a rate of 5 K/min from above its melting point and held at the desired temperature. For temperatures below 225 K, the glass was first annealed at 225 K for approximately 24 h and then cooled further at a rate of 0.3 K/min. This procedure minimized fractures in the glass caused by thermal contraction, avoiding scattered infrared light.

DOI: 10.1021/acs.jpcb.7b08301
J. Phys. Chem. B 2017, 121, 10417−10428

II.II. FT-IR Spectroscopy. FT-IR experiments were performed with a Nicolet 6700 FT-IR spectrometer (Thermo-Fisher Scientific) at 1 cm^{-1} resolution. Temperature-dependent spectra of the PhSeCN in OTP solution were acquired to quantify how the nitrile stretch of PhSeCN evolved with decreasing temperature. OTP has minimal absorption in the vicinity of the CN stretch of PhSeCN (between 2130 and 2170 cm^{-1}), so the peak could be observed directly. Scattered light from fractures in the glass created a mild frequency-independent offset that grew with decreasing temperature. The line shapes were fit with a Gaussian line shape function to obtain peak positions and full width at half-maximum (FWHM).

II.III. Polarization-Selective Pump-Probe Spectroscopy. The methods and equipment used in the ultrafast infrared experiments have been previously described in detail.[20,32] Briefly, a Ti:sapphire oscillator and regenerative amplifier produced ultrafast pulses at 800 nm, which then pumped an optical parametric amplifier that converted the light to the mid-IR (4.6 μm). The IR pulses had energies of a few microjoules, a 1 kHz repetition rate, and were nearly transform limited with a bandwidth of 90 cm^{-1}. The pulse times were controlled to the accuracy of <0.1 fs with mechanical delay stages. The delay stages give a maximum time delay of ~2 ns.

In polarization-selective pump-probe (PSPP) experiments, each pulse is split into a strong pump pulse and a weak probe pulse. The two pulses are crossed in the sample, and the probe pulse is dispersed on a monochromator and collected on a 32 element mercury−cadmium−telluride array detector. The intensity of the signal with respect to frequency and probe delay time is then measured on the detector. The polarization of the probe is rotated to be either parallel or perpendicular to the polarization of the pump pulse to determine the signals $I_{\parallel}(t)$ and $I_{\perp}(t)$.

The intensities of the parallel and perpendicular polarized decays are given by[30]

$$I_{\parallel} = P(t)(1 + 0.8C_2(t))$$
$$I_{\perp} = P(t)(1-0.4C_2(t)) \quad (1)$$

where $P(t)$ is the isotropic vibrational population relaxation, and $C_2(t)$ is the second Legendre polynomial correlation function, which is the correlation function for the orientational relaxation. Solving the system of equations yields

$$P(t) = \frac{I_{\parallel} + 2I_{\perp}}{3} \quad (2)$$

$$r(t) = 0.4C_2(t) = \frac{I_{\parallel} - I_{\perp}}{I_{\parallel} + 2I_{\perp}} \quad (3)$$

The excited population relaxation is exponential in time in the absence of population transfer mechanisms. Although it is possible for the anisotropic decay, $r(t)$, to be single exponential, which corresponds to a single, orientationally diffusive process, it is common to see multiexponential decays as well. This can be most simply understood in terms of the "wobbling-in-a-cone" model, where a fast diffusive process is limited to motion within a cone of a certain angle.[33−35] A slow diffusive process is then responsible for reorienting the fast cone throughout the rest of the angular space.

The anisotropic decay, $r(t)$, also has a deviation from its maximum value of 0.4 at very short times, typically <100 fs. The deviation arises from ultrafast inertial orientational motions that are too fast to be measured with the pulse durations used in the experiments.[36] The inertial motion can be similarly understood in terms of a restricted-angle orientational process. The complete model can then be written explicitly for a biexponential decay as

$$C_2(t) = T^2(S^2 + (1 - S^2)\exp(-t/\tau_1))\exp(-t/\tau_2) \quad (4)$$

where T and S are order parameters of the inertial and diffusive cone, respectively. They have the generic form

$$Q = \frac{1}{2}\cos\theta_0(1 - \cos\theta_0) \quad (5)$$

where θ_0 is the half angle of the cone for each restricted angular process.

II.IV. Two-Dimensional IR Vibrational Echo Spectroscopy. For vibrational echo experiments, each mid-IR pulse is split into four pulses. The first three pulses of approximately equal intensity are overlapped spatially in the sample. This generates a vibrational echo signal that propagates in an independent direction. The fourth weaker pulse serves as a local oscillator (LO), which is overlapped spatially and temporally with the echo prior to the array detector to provide heterodyne signal amplification and phase information.

The delay time (τ) between pulses 1 and 2 is scanned while holding the delay time (T_w) between pulses 2 and 3 constant. This generates a time-domain interferogram on each of the array pixels. Numerical Fourier transforms of the interferograms at each pixel frequency give the complete 2D IR spectra at a given T_w, with the vertical axis given by the array spectrograph frequencies and the horizontal axis given by the Fourier transforms of the interferograms.

Qualitatively, the 2D IR experiment works as follows. The echo experiment "labels" the initial frequencies of the vibration of the probe with the first two pulses. During the delay time T_w, the structure of the sample evolves, which can cause spectral diffusion to occur. Pulse 3 creates the final echo signal, which reports on the final frequencies of the probe vibration. The 2D spectrum then shows the correlation between the initial frequencies ω_τ with the final frequencies ω_m at a given waiting time T_w. If the waiting time is short with respect to the time scale of complete spectral diffusion, which is the case in the glass phase, then the 2D spectrum looks elongated along the diagonal, indicating a high correlation between initial and final frequency. If the waiting time is much longer than the time scale of spectral diffusion, then the spectrum becomes rounder, indicating a decorrelation between the initial and final frequencies. The correlation can then be quantified through the center line slope (CLS) method,[37,38] which yields the normalized frequency−frequency correlation function (FFCF). Briefly, the CLS method is calculated by taking slices of the 2D spectrum parallel to one of the frequency axes, finding the maximum of each slice, and fitting a line through the maxima. The slope of the fitted line is the value of the CLS for the spectrum. A plot of the CLS at each T_w, i.e., the CLS(T_w), is the CLS decay, the normalized FFCF.

The FFCF, which quantifies spectral diffusion, is the probability that an oscillator at a given frequency will have that same frequency at a later time, averaged over the entire inhomogeneous line shape. The FFCF can be modeled with a simplified Kubo form[39]

DOI: 10.1021/acs.jpcb.7b08301
J. Phys. Chem. B 2017, 121, 10417−10428

$$C(t) = \langle \delta\omega(0)\delta\omega(t)\rangle = \sum_i \Delta_i^2 \exp(-t/\tau_i) \quad (6)$$

Where the Δ_i are the frequency amplitudes (range of frequencies sampled) and τ_i is the associated characteristic time scale. The Kubo line shape has the property that any component where $\Delta_i\tau_i < 1$ is "motionally narrowed" and is a source of homogeneous broadening. The frequency amplitude and time scale of a motionally narrowed component cannot be determined separately but can only be resolved as part of the pure dephasing line width

$$\Gamma^* = \frac{\Delta^2\tau}{\pi} = \frac{1}{\pi T_2^*} \quad (7)$$

Where T_2^* is the pure dephasing time. The observed homogeneous dephasing time T_2 has additional contributions from the vibrational lifetime and the orientational relaxation, which are neglected here as both are much longer than the pure dephasing time at all temperatures studied. The homogeneous components cause the deviation from the theoretical maximum value of 1 in the CLS(T_w).

In the glass phase, the tau scan interferograms become extremely long, with the scan at 100 K being in excess of 100 ps in length due to the large increase in the dephasing time, T_2. Sampling at the Nyquist rate in the stationary frame requires a 4 fs step size. A single interferogram would then require over 25 000 steps to acquire and take over 6 h. By taking the data in a rotating frame,[40] the sampling rate was decreased to 200 fs intervals, greatly increasing the data acquisition rate. For the coldest temperatures, the interferogram was apodized, i.e., multiplied by a rapidly decaying Hann function, to artificially shorten the scan to ~25 ps in length. Performing the CLS analysis along the ω_τ axis provides accurate results with heavy apodization, as has been demonstrated previously.[37] Note when the CLS is performed along the ω_m acquired with a monochromator, apodization will distort the results.[37,38] As the anharmonicity between the 0−1 and 1−2 vibrational transition is much larger than the FWHM of the absorption, the two techniques give identical results in the absence of apodization. The use of apodization further shortened the required length of the tau scan, which increased the rate of data acquisition.

As the local oscillator and the echo signal are overlapped spatially and temporally to determine the full 2D line shape, small differences in chirp and alignment can have significant impact on the calculated CLS value for highly correlated line shapes. Although the time evolution of the CLS is conserved, this can affect the calculated frequency amplitudes and homogeneous dephasing time. This can be largely mitigated through "phasing" the data to have the projection of the absorptive line shape on the ω_m axis match that of the PSPP data. Additional checks involve phasing to have the CLS ω_m and CLS ω_τ calculations match within experimental error at all T_ws in the absence of apodization (corresponding to data taken at temperatures above 200 K), as most common distortions cause the calculations to deviate in the opposite manner.

The dephasing time, T_2, can be obtained independent of the CLS, which also allows for the determination of the expected starting point of the normalized CLS decay. The resonant frequency-resolved rephasing interferogram can be shown to decay, in the absence of spectral diffusion, that is, with $T_w \sim 0$, as

$$S(t) \propto \exp\left(-\frac{t}{T_2/2}\right) \quad (8)$$

Equation 8 is the field equivalent of the intensity measurements made in two-pulse echo experiments.[41]

The 2D IR experiment is very sensitive to scattered light. Despite efforts to mitigate thermal contraction-induced fractures in the glass, at the lowest temperatures, the scattered light could be of greater intensity than that of the local oscillator. Although optical chopping of pulse 3 enables subtraction of the majority of the scattered light, it was necessary to employ a four-step phase cycling procedure to both subtract scattered light and remove scatter that was heterodyned with the chopped pulse.[42] An analogous two-step procedure was used to remove scatter from the pump-probe decays as well.

III. RESULTS AND DISCUSSION

III.I. FT-IR Spectroscopy. Temperature-dependent FT-IR spectra were obtained for PhSeCN in OTP from above T_m to 100 K, nearly 150 K below T_g. Representative spectra can be seen in Figure 1. Throughout the liquid phase to about 40 K below the glass transition temperature, the peak remained centered at ~2155 cm^{-1} with an FWHM of about 9 cm^{-1}. From 200 to 100 K, the spectrum peak shifted slightly to 2156 cm^{-1} and its FWHM increased by 1 cm^{-1}. The very small changes in the spectra with temperature show that the range of environments experienced by the vibrational probe do not change significantly between the liquid and the glass.

III.II. 2D IR Vibrational Echo. Two-dimensional IR vibrational echoes were taken for a range of temperatures extending from slightly above the glass transition to 100 K, nearly 150 K below T_g. Several of the CLS(T_w) (normalized FFCF) curves for this temperature range are shown in Figure 2. These 2D IR data are combined with data taken in the liquid and supercooled liquid temperature ranges reported previously.[24]

It is important to note that the CLS decays did not change with aging. Holding the sample at a temperature slightly below T_g (225 K) and monitoring the CLS of a particular T_w showed no trend over a period of 15 h. Further, holding the sample below T_g for a period of approximately a week yielded no detectable change in the observed decay. These results are shown in Figure 3. The absence of changes with aging demonstrates that the decay is only sensitive to the absolute temperature and not the thermal history of the material, which is significantly different from slow relaxation processes associated with diffusion.[3]

As in the previous work,[24] the decays were fit (solid lines in Figure 2) using the Kubo line shape model. The Kubo model (eq 6) describes the FFCF as a sum of exponentials plus a constant offset, where the offset corresponds to relaxations that are on timescales longer than can be measured in the experimental window, which is limited by the probe vibrational lifetime. The complete set of FFCF parameters for PhSeCN in glassy OTP are given in Table 1. In the liquid phase, as reported and discussed in detail previously,[24] the CLS decays required two or three exponential decays to fit the data, depending on the temperature. As the temperature was decreased, the longest of the decays was pushed beyond the experimental window and the third exponential became an offset to a biexponential decay.

DOI: 10.1021/acs.jpcb.7b08301
J. Phys. Chem. B 2017, 121, 10417−10428

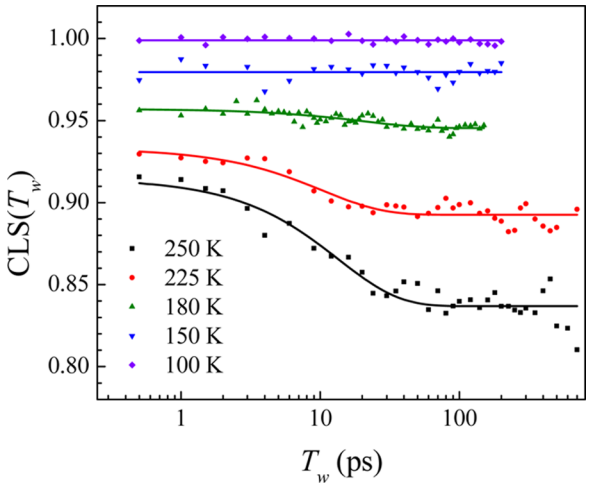

Figure 2. CLS decay (normalized frequency−frequency correlation function) for PhSeCN in OTP at a variety of temperatures near and below the glass transition. The solid lines are fits with a single exponential decay to an offset. The decreasing homogeneous component (difference from 1 at T_w = 0) and increasing inhomogeneous offset are clearly visible. The fast component can be seen to decrease in amplitude and increase in time scale before becoming indistinguishable between 150 and 180 K.

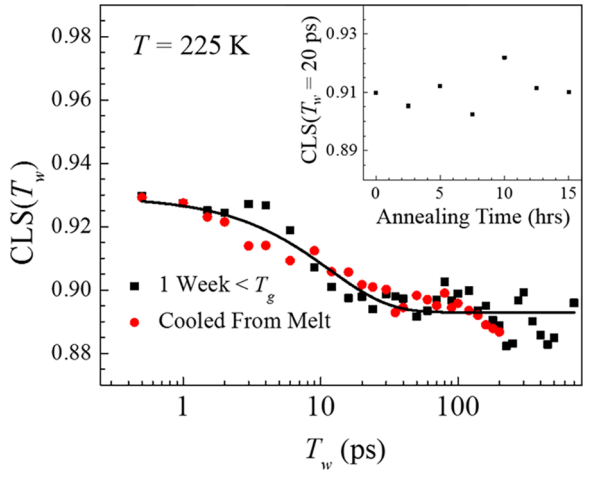

Figure 3. CLS decay of PhSeCN in OTP at 225 K for a freshly cooled sample (red circles) compared to a sample that has been kept below T_g for over 1 week (black squares). Their agreement shows that the CLS decay is independent of the thermal history of the material and only depends on the absolute temperature. Inset: The CLS point at 20 ps monitored over a period of 15 h, showing no time-dependent change on the hours time scale.

Near T_g, only a single exponential decay with a large offset was observed and was measurable to 60 K below the glass transition. Unlike the slow decay processes, which become an offset in the CLS decay due to becoming much slower than the experimental time window, the fast decay disappears due to its amplitude dropping exponentially with decreasing temperature. As the overall inhomogeneous line width of the spectrum increases slightly as the temperature decreases, this means the range of frequencies (structural configuration) that are sampled by the fast process at higher temperatures can only be sampled through slow, diffusive processes at lower temperatures. This qualitative behavior, weakly increasing time scale and sharply decreasing amplitude with decreasing temperature, is similar to previous observations of fast processes in OTP.[7,8,14]

The time constants (τ_1) and amplitudes (frequency fluctuation range) (Δ_1) of the fast process with respect to temperature are displayed in Figure 4, including the data for the fast process in the liquid phase. Both terms show a clear Arrhenius temperature dependence over the 180 K range studied (solid curve fits), corresponding to an activation energy of 3.3 ± 0.2 kJ/mol. The temperature dependence of the relaxation rate is unbroken through the glass transition, showing the continuity of the process from the liquid to the glass phase. An important feature of the data is that the frequency amplitude, Δ_1, decreases with decreasing temperature in precisely the opposite manner as the time constant, τ_1, such that the dimensionless (s rad/s) constant $\Delta_1\tau_1$ is independent of the temperature above and below T_g.

Although $\Delta_1\tau_1$ is independent of temperature in each phase, a step discontinuity in its value occurs between the liquid and the glass. The value goes from 2.70 ± 0.06 in the liquid to 1.70 ± 0.06 in the glass, a decrease of nearly 40%, which is well outside of the range of error. The decay time is continuous with respect to temperature within experimental error, but a sudden drop in the frequency amplitude occurs at the glass transition.

The abrupt drop in $\Delta_1\tau_1$ is unusual; it does not have an analogue in previous studies of ultrafast motions in glass formers. $\Delta_1\tau_1$ is temperature independent above and below the glass transition. The discontinuity is only in the frequency amplitude; the characteristic time scale of the fast motion is continuous across the glass transition region. As it is generally believed that microscopic motions are similar between the liquid and the glass phase, this continuity in time scale is consistent with general conceptions of microscopic fast processes near the glass transition.

In addition to the ultrafast spectral diffusion, the FFCF has a motionally narrowed homogeneous component in the glass and liquid phases. The homogeneous component (Γ in Table 1) is in part made up of motions that sample a range of frequencies very fast compared to the inverse of the frequency range, such

Table 1. FFCF Parameters for PhSeCN in Glassy OTP

T (K)	T_2 (ps)	Γ (cm^{-1})	Δ_1 (cm^{-1})	τ_1 (ps)	Δ_2 (cm^{-1})
250	8.6 ± 0.1	1.23 ± 0.01	1.08 ± 0.04	13.5 ± 1.8	3.74 ± 0.02
235	10.0 ± 0.4	1.06 ± 0.04	0.77 ± 0.04	11.5 ± 2.5	3.87 ± 0.01
225	11.6 ± 0.3	0.91 ± 0.03	0.72 ± 0.04	12.9 ± 2.3	3.87 ± 0.02
210	12.6 ± 0.1	0.84 ± 0.01	0.51 ± 0.03	13.8 ± 3.4	3.94 ± 0.02
200	14.0 ± 0.4	0.75 ± 0.02	0.60 ± 0.01	14.5 ± 2.3	3.92 ± 0.02
180	17.0 ± 0.2	0.62 ± 0.01	0.41 ± 0.03	20.2 ± 5.5	4.32 ± 0.01
150	30.0 ± 0.6	0.35 ± 0.01			4.34 ± 0.01
100	64.0 ± 0.4	0.165 ± 0.001			4.42 ± 0.01

DOI: 10.1021/acs.jpcb.7b08301
J. Phys. Chem. B 2017, 121, 10417−10428

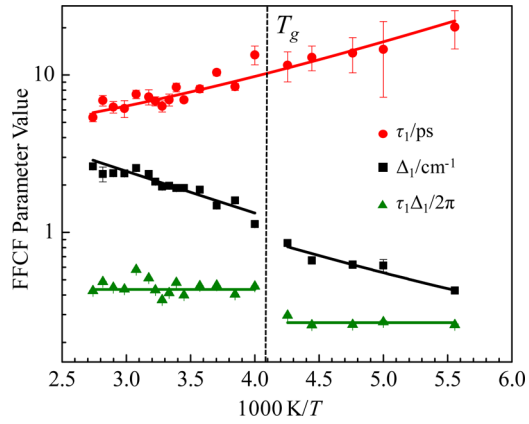

Figure 4. Arrhenius plot of the CLS fast time constant (in ps, red circles) and frequency amplitude (in cm^{-1}, black squares) measured in PhSeCN in OTP, including data from the liquid phase.[24] Also plotted is their corresponding dimensionless product (in s rad/s, green triangles), offset by a factor of 2π for clarity. The time constants and amplitudes have Arrhenius temperature dependencies (solid lines) that are the inverse of each other such that their product is generally temperature independent. A discontinuity occurs at the glass transition, where the amplitude suddenly decreases, but otherwise maintains the same temperature dependence, causing the product to jump to a smaller constant in the glass phase.

that the product $\Delta\tau < 1$. The temperature-dependent dephasing time (T_2), corresponding to the inverse of the homogeneous line width, has been previously well described with a variety of glass formers with a variety of probes using infrared two-pulse photon echo experiments.[41,43]

The observed temperature dependence of T_2 of PhSeCN in OTP can be fit well to a T^{α} power law with $\alpha = 2.35$ in the glass and supercooled phases (Figure 5). An $\alpha \approx 2$ power law can correspond to dephasing caused by two-phonon scattering processes between potential wells in glasses,[41] which is commonly seen in electronic dephasing[44] in high-temperature glasses and has been seen in vibrational spectroscopy with tungsten hexacarbonyl ($W(CO)_6$) in a variety of glass formers.[43] At very high temperatures, this power law breaks down, which is again analogous to the previous studies. This change in $W(CO)_6$ was previously attributed to its triply degenerate vibrational modes splitting differently in glassy and

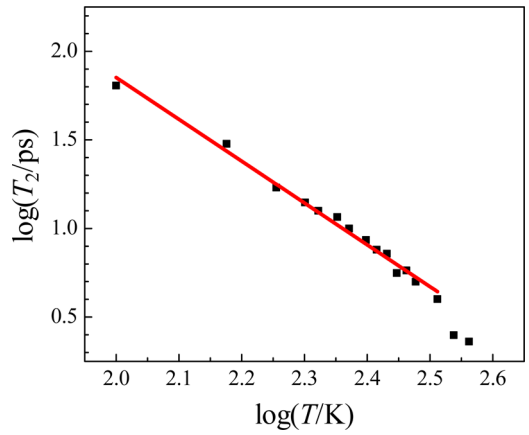

Figure 5. Dephasing time (T_2) vs temperature for OTP in the liquid and glass phase. Solid line corresponds to a power law with exponent 2.35.

liquid environments.[43] The fact that the same trend is seen in the nondegenerate nitrile stretch of PhSeCN suggests that it is a more fundamental property of vibrational dephasing in glasses in the absence of a thermally activated dephasing mechanism. A likely source of the deviation from the power law at high temperatures is additional motionally narrowed dynamics that are too slow at lower temperature to be a component of the homogeneous line width. These dynamics would appear as spectral diffusion at lower temperatures.

The remaining inhomogeneous component (Δ_2 in Table 1) becomes larger with decreasing temperature as the homogeneous component and the fast component become a smaller fraction of the total absorption spectrum. This large Δ_2 component is connected to the variety of diffusive motions that are resolvable for most of the liquid phase within the 1 ns experimental window, but occur on extremely long timescales in the glass phase. A thorough description of the liquid phase behavior of this component can be found in a prior publication.[24]

In summary, the CLS decay (spectral diffusion) near T_g is well described by an exponential decay going to a large offset, where the exponential process describes a set of fast molecular motions and the offset corresponds to substantially slower motions. The dephasing time T_2 increases smoothly with decreasing temperature with approximately a T^2 power law, causing the homogeneous line width to approach zero and the initial CLS value to approach one. The fast motion's amplitude (Δ_1) decreases and its time constant (τ_1) increases in an Arrhenius manner, with an identical activation energy of 3.3 kJ/mol. However, there is an anomalous, discontinuous jump in the frequency amplitude at T_g that causes the otherwise temperature-independent product $\Delta_1\tau_1$ to drop by 40%. A model for this behavior is presented below.

III.III. Infrared PSPP Spectroscopy. To better understand the origin of the observed fast motions in the 2D IR data, PSPP data were taken for the OTP system at a number of temperatures in the liquid and glass phases. Using eqs 2 and 3, the acquired parallel and perpendicular polarized decays were combined into their isotropic and anisotropic components.

The isotropic decay is the decay of the excited state population back to the ground state (vibrational lifetime). For PhSeCN in OTP, this decay is single exponential with a lifetime (T_1, see Table 2) of approximately 450 ps. This lifetime has a mild dependence on both wavelength and temperature, varying between 420 and 480 ps over the range studied. The vibrational lifetime seen for other nondegenerate vibrational modes in glass forming liquids have previously been found to be largely temperature independent. For example, the asymmetric CO stretch of $Rh(CO)_2$acac in dibutyl phthalate increases by only 10% from room temperature to 3.5 K.[43]

No strong wavelength dependence was observed for the anisotropic relaxation near the center of the line shape, the same as in the population decay. The anisotropic decay captures the dipole reorientation time (orientational relaxa-

Table 2. Wobbling-in-a-Cone Analysis for PSPP of PhSeCN in OTP

T (K)	T_1 (ps)	θ_{in} (deg)	θ_1 (deg)	τ_1 (ps)	τ_2 (ps)
325	430 ± 5	15 ± 1	30 ± 1	16 ± 1	215 ± 8
300	461 ± 3	19 ± 3	28 ± 2	32 ± 11	830 ± 120
225	477 ± 5	13 ± 7	20 ± 3	370 ± 280	

DOI: 10.1021/acs.jpcb.7b08301
J. Phys. Chem. B 2017, 121, 10417−10428

tion); it displays a strong temperature dependence. Two representative decays are shown in Figure 6 for the PhSeCN in the liquid and the glass phase. As can be seen, even at room temperature the OTP reorientation time is very long, requiring more than the nanosecond of the experimental window to fully randomize its orientation, that is, for the anisotropy, $r(t)$, to decay to zero. In the glass phase, reorientation is extremely slow. A best fit with a single exponential to an offset predicts a low-amplitude reorientational process that takes several hundred picoseconds to complete, but the poor signal-to-noise at late time makes it difficult to describe precisely. Both anisotropic decays clearly have multiple decay processes, suggesting the use of the wobbling-in-a-cone model described in Section II.III.

The wobbling model (eq 4) used to describe the orientational relaxation of the dipole is composed of an "inertial" cone, which corresponds to <100 fs time scale motions that are substantially faster than can be measured (θ_{in}, corresponding to order parameter T in eq 4); a diffusive cone, which corresponds to restricted-angle orientational diffusion (τ_1 and θ_1, corresponding to order parameter S); and a slow, final diffusive process, which is the time for complete orientation randomization (τ_2). The calculated fit parameters for the wobbling model are given in Table 2. This final time scale generally scales with the viscosity of the liquid described by the Debye–Stokes–Einstein relation, and thus becomes extremely long with decreasing temperature.[22,45] In the glass phase, where viscosity is $>10^{12}$ times higher than at room temperature, this process appears as a constant offset during the experimental window of ∼1 ns.

The diffusive cone has a characteristic time scale (τ_1) that increases with decreasing temperature but at a much slower rate than the final diffusive process. The angle of the cone (θ_1) also becomes smaller, going from ∼30 to ∼20°, indicating more restricted motion, as the glass transition is approached. The slowing as the glass transition is approached and passed through is akin to the spectral diffusion observed with 2D IR; however, the time scale of the 2D IR fast process at glassy temperatures is about 10 times faster than the probe angular motions. The significant difference in timescales indicates that restricted-angle orientational diffusion is not responsible for the observed CLS decay. Although the PhSeCN angular motions are too slow to contribute to spectral diffusion, it is possible that the bulk OTP liquid and glass undergo small-angle reorientations on fast timescales, whereas the vibrational probe does not. However, this seems highly unlikely. The PhSeCN probe is both less massive and takes up less volume than OTP, suggesting that for steric reasons the probe should undergo more rapid angular motions than OTP.

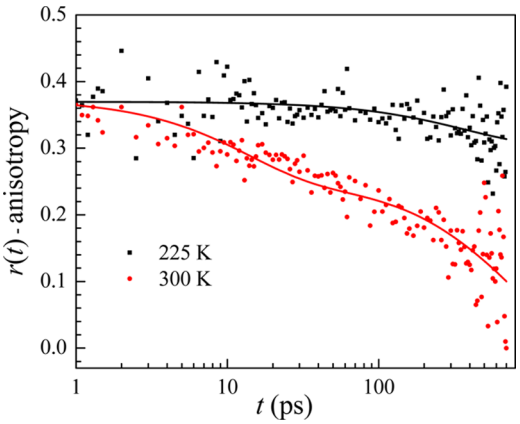

Figure 6. Anisotropic decays from PSPP experiments on PhSeCN in OTP at representative temperatures, describing the orientational relaxation of the nitrile dipole of PhSeCN, fit with multiexponential decays (solid lines). The time scale of orientational relaxation is much slower than that observed in the spectral diffusion.

The PSPP experiments suggest that the dynamics seen in the 2D IR echo experiments are not caused by orientational motions in the liquid and glass. For a hindered rotational process to impact spectral diffusion directly, it must occur on a faster time scale or at least on a comparable time scale to the spectral diffusion.[46] For this reason, both the diffusive cone motions, which are an order of magnitude slower than the CLS decay, and the inertial cone motions, which are orders of magnitude faster than the CLS decay, cannot be the physical origin of the observed process. This suggests that the origin of the spectral diffusion is principally density fluctuations.

III.IV. Brief Comparison to Known Glassy Dynamics and MCT Models. As was established in the previous section, the observed picosecond time scale dynamics appear to originate from density fluctuations. Because the dynamics are far too fast and produce minimal structural randomization, as described by the FFCF, diffusive motions such as the α-relaxation or Johari–Goldstein relaxation can be immediately ruled out. Other elements of the FFCF in the higher temperature liquid can be better associated with these dynamics and are discussed in detail in a previous publication.[24] The boson peak,[1] which is produced by an ultrafast process, might be considered as associated with the dynamics observed here. However, the boson peak is generally observed as arising from a time scale of <1 ps and has little or no temperature dependence. This time scale is more than an order of magnitude faster than the dynamics measured in the current experiments. Furthermore, in the time domain, the boson peak appears as underdamped coherent oscillations,[47] which does not describe the dynamics observed here. The fast β-process predicted by mode coupling theory (MCT) can also be considered as a source of the observed dynamics.

The MCT correlators were originally developed to describe the intermediate scattering function of a hard sphere liquid.[16] Asymptotic analysis of approximations to the exact fluid mechanical equations yielded the characteristic two-step decay functions, where the liquid first undergoes caged, nondiffusive motions before final diffusive randomization. Most of the past measurements of picosecond time scale dynamics in OTP have been interpreted in terms of an MCT fast β-process,[6−9,11,14] so it is worth comparing the observed fast spectral diffusion data to an MCT description.

A principle prediction of MCT is that the first part of the two-step decay (the fast β-process) is characterized by a wave-vector independent, power law decay in time, multiplied by a temperature and wave-vector dependent amplitude, such that

$$F(\vec{q}, t) = f(\vec{q}) + H(\vec{q})G(t) \quad (9)$$

The power laws can be determined directly through a nontrivial calculation from the static structure factor.[16] For OTP, the early time power law exponent has been found to be $a \approx 0.3$.[6,8,9,14]

Although no complete theory of spectral diffusion in vibrational probes exist, analytical approximations are applicable to the case where reorientations can be neglected, i.e., the frequency only depends on changes in interparticle distan-

DOI: 10.1021/acs.jpcb.7b08301
J. Phys. Chem. B 2017, 121, 10417−10428

ces.[48,49] As the MCT power law for the intermediate structure factor is separable in time and space, the power law in time is conserved over the spatial integrals in the analytic FFCF expressions. Thus, the characteristic behavior in time for the fast β-process predicted by MCT should also appear in the spectral diffusion data, provided the assumptions on the analytic approximation are valid. Some of the predictions of MCT can then be compared to the 2D IR data, even though the amplitudes are washed out in the complex spatial integrals.

In general, it is found that a power law decay does not describe the CLS decays. However, due to the nature of the MCT solutions, assessing their suitability is difficult. The power law decays are an asymptotic solution to the MCT equations, meaning they have a narrow range of applicability, excluding very early time and the final exponential decay. In addition, different power laws are predicted for entering and exiting the plateau region of the two-step decay.

For the data taken near and directly below the glass transition, it appears as if the CLS is a decay entering a plateau. This decay should then relate to the experimental $a \approx 0.3$ MCT power law for the fast β-process entering the plateau. However, the power law fit systematically misses the experimental data, regardless of the starting point of the fit. The power law fit is compared to the single exponential fit used in Section III.II in Figure 7 for $T = 250$ K data. Extended MCT correlators, which modify the ideal MCT equations to accommodate lower temperature regimes,[9,15] also did not improve the quality of the fit. The extended MCT adds a small "hopping" perturbation that permits a long-time decay to occur in the β correlator. Reasonable values for the hopping perturbation did not significantly alter the dynamics at short times.

Therefore, the fast spectral diffusion seen in glassy OTP cannot be directly associated with the fast β-process predicted by MCT. This could occur for a number of reasons. The assumptions allowing for the separation of the $G(t)$ term in eq 9 from the FFCF could not be met, causing the CLS decay to have a different coupling to the MCT correlators. In this vein, there has been some success in fitting 2D IR data of liquid crystals with a more complex, three-correlator schematic MCT.[23] The correlator describing the 2D IR data in this case

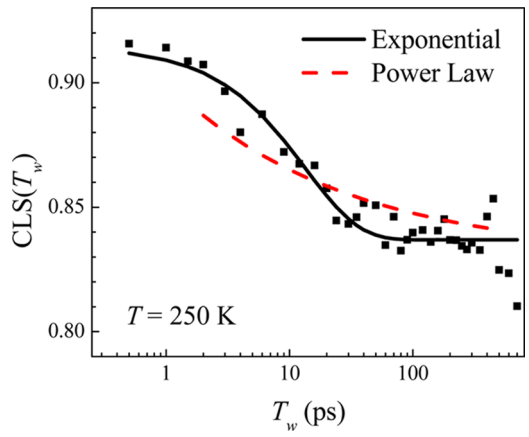

Figure 7. Best fits of exponential and MCT power law decays for PhSeCN in OTP at 250 K. The MCT power law exponent was set to ~0.3, the experimentally measured value, and the constant offset was assumed to be approximately the same as the exponential fit. The poor quality of the power law fit shows that the asymptotic scaling laws of MCT do not adequately describe the 2D IR data.

was associated with large wave-vector (short distance) density fluctuations. This sort of motion is not dissimilar from the qualitative description of the fast β-process although being quantitatively much more complex. However, deeper physical interpretations of the fits are unclear, and their application to the glass former data is an ongoing effort.

Another possibility is that the true fast β-process is obscured by other characteristic motions of the OTP liquid. The origin of such a masking process has previously been attributed in OTP and similar liquids to vibrational−translational coupling[18,50] and phonon-density fluctuations[17] in several quasielastic scattering studies. However, it is difficult to directly associate these processes with processes that would appear as spectral diffusion.

III.V. Potential Energy Landscape (PEL) Model. *III.V.I. Description of the Model.* To help understand the temperature dependence nature of the fast spectral diffusion dynamics, a simple potential energy landscape (PEL) model was constructed that replicates the key experimental results. The potential energy landscape of glass forming liquids has been conceptualized as being very rough, with a fine structure made up of many potential energy minima.[1−4,31,51−54] The local "roughness" of the potential energy landscape is made up of many minima separated by relatively small energy barriers that correspond to small-scale fluctuations in the liquid, whereas large diffusive motion corresponds to motion from one of these corrugated "rough" basins to a neighboring basin.

As these diffusive motions operate on a time scale that is much longer than the microscopic motion, especially in the glassy and deeply supercooled regimes, we can limit our potential energy basin to a single well, which is taken to be quadratic to the lowest order. In the model, the complex high dimensionality potential is modeled as one dimensional, which is sufficient to illustrate the basic features.

A comparison can be drawn to the tunneling two-level systems (TLSs) that can be used to describe the heat capacity, dynamics, and other properties of extremely low-temperature glasses.[55−57] In a low-temperature glass, the potential surface has a high dimensionality but it is assumed that the system is in a local minimum and there is only a single other minimum that is separated from the initial state by a low enough barrier to be accessible at a given temperature. This multidimensional system is reduced to a collection of one-dimensional systems.

In the liquid and glass near T_g, the potential energy surface on which molecular dynamics occur is also of very high dimensionality, which is here reduced to a one-dimensional potential. At these higher temperatures, dynamics occur by going over barriers rather than tunneling through them. The model one-dimensional well has a corrugated surface made up of peaks of roughly equal amplitude. This potential energy surface is given by

$$V(x) = ax^2 + b(1 - \cos(2\pi x)) \tag{10}$$

where a describes the steepness of the well and b describes the height of the small energy barriers. An illustration of the potential energy surface is given in Figure 8. This model surface should be taken as the "fine structure" in the much deeper wells employed in most other treatments of the potential energy landscape.[1−4,31,51−54] The fine structure in the current model gives rise to the fast, nondiffusive motions.

Similarly, we are not interested in motion within one of the small fine structure wells, which would be on a much faster time scale, so we only care about which of the small wells the system

DOI: 10.1021/acs.jpcb.7b08301
J. Phys. Chem. B 2017, 121, 10417−10428

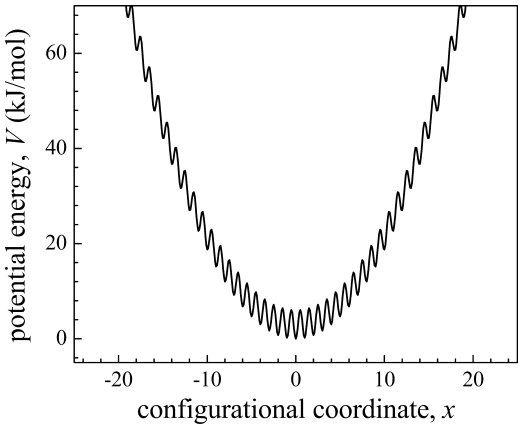

Figure 8. Corrugated potential well model used to describe the observed characteristics of the fast component of the CLS decay. This potential represents the fine structure in the much deeper wells of other treatments of the potential energy landscape. Moving to a neighboring potential well corresponds to small change in the liquid structure with a corresponding small change in resonant frequency for the probe. As the temperature is increased, the liquid can both sample wells at a faster rate and sample a larger number of wells.

is in at a particular time. This allows us to discretize our potential energy surface to just the well minima.

Motion on the surface can then be described by a random walk on a Markov chain, where the probability of moving to the neighboring well in a given time step is given by the rate of crossing the energy barrier.[58,59] With a sufficiently high barrier, the probability of taking a step is exponential in time and the probability of remaining in the well is one minus the probability of taking a step. The exponential rate constant for a given temperature is given by an Arrhenius equation. Then, the probability of crossing a barrier after a given time is

$$P_0 = 1 - \exp[-k \exp(-\Delta V/kT)] \quad (11)$$

where k is the Arrhenius prefactor. The value of k is in part determined by the number of microstates available to the random walk. ΔV and k are ultimately determined by the temperature-dependent experimental data. The probability of going over the left or right barrier is treated as a weighted average, where the probability of staying in the original well is the same as the probability of not crossing the lower barrier, as per eq 11.

The position along the well is described in terms of an idealized configurational coordinate, x, that models the multidimensional configurational system as one dimensional. The change of frequency, $\delta\omega$, of the probe is then also a function of this coordinate. By construction, $\delta\omega$ has zero mean, so $\delta\omega$ is an odd function of x. As we are only looking at small fluctuations around the mean in $\delta\omega$, we construct it as a power series to order x^3

$$\delta\omega(x) = c(x + gx^3) \quad (12)$$

where $g < 1$ and c is a scaling coefficient that sets the range of frequencies sampled. It is adjusted to match the experimental results.

III.V.II. Results from the PEL Model. Random walks were simulated on the Markov chain at a variety of values of kT for a number of different parameters. The calculated FFCF, $\langle\delta\omega(0)\delta\omega(t)\rangle$, was found to have an exponential decay. For a range of kT, which varied from roughly a quarter to two-thirds of the potential energy barrier height, the standard deviation, Δ, and characteristic time scale, τ, of the FFCF had exactly opposite Arrhenius temperature dependence such that their product is essentially independent of temperature, replicating a key experimental finding. Figure 9 displays representative FFCFs (A) and calculated parameters scaled to the experimental data (B). The height of the small energy barriers was found to be ~6 kJ/mol, about double the corresponding experimental activation energy of the FFCF.

The results shown in Figure 9B proved to be robust within the experimental temperature range for a wide range of parameters. At lower temperatures, the characteristic time scale grew faster than the standard deviation due to the very low number of wells involved in the walk. At sufficiently high temperature, kT is much greater than the small barriers between microstates. The motion on the potential surface becomes essentially motion on a smooth parabolic surface. The model of a walk among microstates is no longer applicable. The energy scale is set by the parameter b in the potential energy surface equation (eq 10); it rescales which kTs are in the "valid"

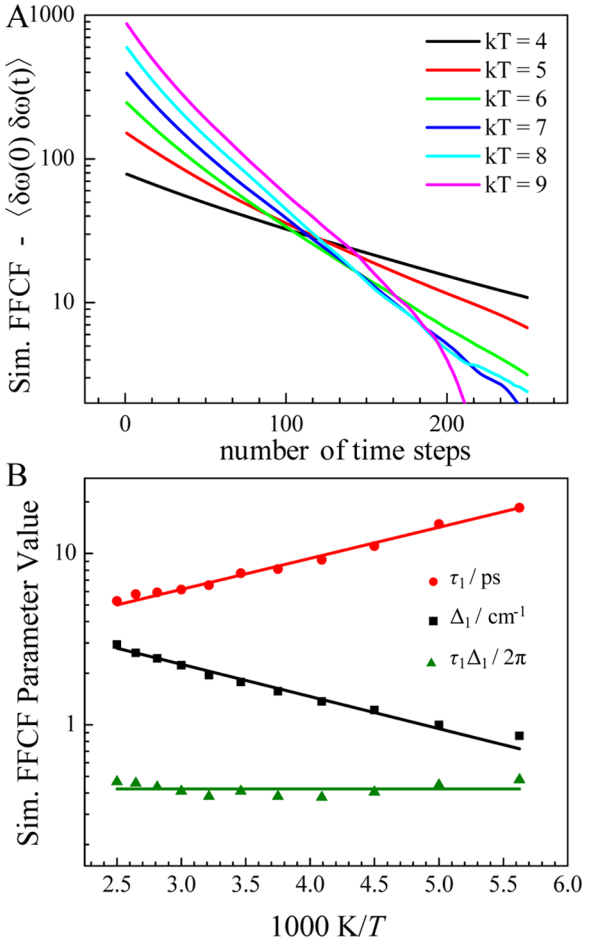

Figure 9. (A) Calculated autocorrelation functions for the frequency function for the corrugated potential model at a range of temperatures. They are well described as exponential decays, and show the desired property of increasing in amplitude while decreasing in characteristic time scale. (B) The time scale and standard deviation of the frequency autocorrelation function and their product scaled to match the liquid phase 2D IR data from Figure 4. Although the simple model cannot explain the discontinuity at T_g without changes to parameters, the other temperature-dependent properties appear readily.

DOI: 10.1021/acs.jpcb.7b08301
J. Phys. Chem. B 2017, 121, 10417−10428

regime. The steepness of the large well, given by the parameter a, controls the number of microstates that are accessible to the biased random walk. The parameter a can be changed by nearly two orders of magnitude without changing the temperature dependence of the FFCF. An excessively steep well gives a small number of microstates available and causes the FFCF to be nonexponential due to large variation in energy barrier heights. For sufficiently shallow wells, increasing the number of wells available proportionally increases how quickly the random walk must move through the potential energy surface to decay on a given time scale. The well steepness was then chosen to give a reasonable value for the microstate interconversion time, assumed to be on approximately the picosecond time scale.

Changing the geometry of the large well by adding cubic or quartic contributions did not significantly alter the basic result. If the parameters were chosen to be large enough so that the well became substantially steeper, i.e., the number of microstates available at higher temperature were substantially decreased, then the predicted energy barrier height between microstates decreased slightly, to around 5 kJ/mol. Significant contributions higher than a quartic were necessary to decrease the barrier more. Given the small energy barriers, a Gaussian distribution of heights also had little impact for a reasonable standard deviation of heights. Increasing the standard deviation to be greater than a quarter of the mean barrier height (∼1.5 kJ/mol) caused the autocorrelation function to become nonexponential. This gives a surprisingly narrow distribution of barriers that reproduce the nature of the experimental data for the model one-dimensional potential energy surface.

The most significant changes in the calculated temperature dependence occur for changes in $\delta\omega(x)$ (eq 12). Having $\delta\omega$ as only linear in x yields an extremely large energy barrier (∼16 kJ/mol), and the valid temperature range where $\Delta\tau$ is a constant occurs at very high temperatures (>400 K). Having the dominant term as cubic in x gives the previously stated smaller energy barrier (∼6 kJ/mol) and a valid temperature range that corresponds to the experimental range. In terms of eq 12, the cubic parameter needs to be only 5% of the linear term to be dominant, provided they have the same sign. A dominant quintic term gives an energy barrier that is similar to that of the quartic energy potential (∼5 kJ/mol) and a relevant temperature range similar to that of the dominant cubic term.

III.V.III. Interpretation of the Discontinuity with the PEL Model. The model presented above be can be used to provide a possible explanation for the experimental discontinuity at the glass transitions. As can be seen by comparing Figure 9B to Figure 4, the discontinuity at T_g does not occur in the model calculations shown in Figure 9B. The discontinuity occurs in the experimentally measured decrease in the standard deviation of the range of frequencies sampled, Δ_1. The decrease is approximately 40%. However, there is no abrupt change in the time constant, τ_1. The discontinuity can be introduced by an abrupt change in parameters. This change can be in either an increase in the steepness of the potential energy surface, i.e., a increases by nearly a factor of 2 in eq 10 or a decrease in the frequency change scaling coefficient, c, in eq 12. A combination of changes in both parameters is also possible.

The former scenario, increasing the slope of the potential well, decreases the number of microstates accessible at a given temperature, and therefore decreases the range of frequencies sampled. This change in the surface seems possible given the loss of degrees of freedom that occurs at the glass transition.[2,4,60−62] However, changing the potential in this manner causes the calculated characteristic time scale to have a discontinuity at T_g as well, which does not match theory or experiment. To avoid this discontinuity, the Arrhenius prefactor k in eq 11 must suddenly decrease by an identical factor. This means the time it takes for the liquid to shift between two microstates suddenly doubles without any significant change in the potential energy landscape near the bottom of the well (see Figure 8). Although this abrupt change seems implausible initially, it could occur because of a sudden change in the entropy difference between microstates when going below the glass transition, such as in the entropy prefactor in the Eyring transition state rate constant equation.[63] However, the perfect balance necessary to avoid a discontinuity in the temperature dependence of the FFCF time constants might make the second scenario more plausible.

In the second scenario, reducing the scaling of $\delta\omega(x)$, c in eq 12, gives the glass access to the same number of microstates but the sampling covers a smaller range of frequencies. This proposal avoids the awkward balancing required by the first scheme, but it is necessary to impart a physical meaning to the rescaling. One possibility again involves the change in the number of degrees of freedom at T_g. There is a main set of degrees of freedom for which thermally induced structural changes takes the system from one microstate to another, resulting in frequency changes. There is a secondary set of degrees of freedom that in the liquid undergo changes when the main set goes from one microstate to another. These also contribute to frequency changes but do not determine the barrier height. In the glass, the secondary set no longer changes when the main set changes microstate. Thus, the secondary set's contribution to frequency change is lost in the glass.

Mathematically, either scenario 1 or 2 can account for the abrupt drop in Δ but a smooth change in τ at the glass transition. The two physical explanations that we have given are trying to account for a phenomenon occurring on a complex multidimensional potential surface in terms of a one-dimensional potential surface model. This should be considered a heuristic attempt to suggest the nature of the processes that might be involved in the observed discontinuity in the data at T_g rather than a robust explanation.

In summary, a random walk on a very simple model 1D potential energy landscape can recreate the basic thermodynamic characteristics exhibited by the fast spectral diffusion in the liquid through the glass transition, namely the inverse temperature dependence of the standard deviation Δ (frequency amplitude) and characteristic time scale τ of the FFCF. With further simple modifications, albeit without correspondingly simple thermodynamic or real space descriptions, the discontinuity in the standard deviation can be recreated in two different manners.

IV. CONCLUDING REMARKS

A fast dynamical process above and below T_g in the glass former OTP was characterized using 2D IR vibrational echo spectroscopy performed on a long lifetime vibrational probe. The 2D IR data gives the frequency−frequency correlation function, which in this case was fit very well as a fast single exponential decay to a nonzero offset. The offset reflects much slower processes that were too slow to measure within the experimental time window. The exponential decay of the fast process had a characteristic time constant that increased and amplitude (range of frequencies sampled) that decreased as the temperature was lowered. The decay time constant and the

DOI: 10.1021/acs.jpcb.7b08301
J. Phys. Chem. B 2017, 121, 10417−10428

amplitude both displayed an Arrhenius temperature dependence with identical activation energies. The product of these two observable quantities yielded a temperature invariant dimensionless quantity above and below T_g. However, the frequency amplitude dropped suddenly at T_g but then continued to decrease with the same activation energy. The drop in the amplitude caused the otherwise temperature invariant product to suddenly decrease by 40% in going through T_g. No equivalent discontinuity has been previously reported at T_g for fast motions in OTP.

IR polarization-selective pump-probe experiments indicate that the origin of the observed fast process is not small-angle reorientations of the liquid, which suggests that the physical origin of the fast process is principally density fluctuations. However, direct application of the asymptotic MCT solutions to the 2D IR data was unsuccessful, indicating that the fast spectral diffusion process is not identically the MCT fast β-process.

The quantitative behavior of the fast process was successfully reproduced with a one-dimensional potential energy surface model. The potential energy surface was modeled as a rough basin, where a large potential energy well, reflecting a broad local minimum, has a fine substructure made up of many small minima. The large well is separated from the next large well by a barrier that is too high to surmount on the experimental time scale. Each minimum is associated with a distinct vibrational transition energy of the vibrational probe. Therefore, motion on the surface causes the vibrational frequency to fluctuate, giving rise to spectral diffusion.

Performing a biased random walk on this energy surface allows the system to sample many minima quickly at high temperatures, and a small number of minima slowly at lower temperatures. Numerical calculations were used to obtain the FFCF, which was compared to the data. Comparison between the model calculations and the data yielded the barrier between the minima on the rough surface to be between 5 and 6 kJ/mol. This model accurately reproduced the temperature-dependent data except for the drop in the frequency amplitude at T_g. By changing the steepness of the potential surface without changing its roughness or changing the coupling between the frequency and the configurational coordinate that gave the position on the surface, the model could also reproduce the discontinuity observed experimentally at T_g.

The discontinuity demonstrates that the fast structural dynamics of the material is sensitive to the passage through the glass transition. Although the time dependence of the frequency fluctuations is continuous through T_g, the range of frequencies sampled is discontinuous. The range of frequencies sampled reflects the range of interconverting structures that are active. The drop in the range of frequencies sampled indicates that a significant fraction of fast structural fluctuations that occur in the liquid suddenly slow substantially at T_g.

AUTHOR INFORMATION

Corresponding Author

*E-mail: fayer@stanford.edu. Tel: 650 723-4446.

ORCID

David J. Hoffman: 0000-0001-8518-7676
Michael D. Fayer: 0000-0002-0021-1815

Notes

The authors declare no competing financial interest.

ACKNOWLEDGMENTS

This work was supported by the Division of Chemistry, Directorate of Mathematical and Physical Sciences, National Science Foundation (NSF) (No. CHE-1461477). We thank P. Kramer and J. Nishida for helpful discussions and R. Yuan for help with the cryostat.

REFERENCES

(1) Donth, E.-J. *The Glass Transition: Relaxation Dynamics in Liquids and Disordered Materials*; Springer: Berlin, 2001; Vol. *48*.

(2) Debenedetti, P. G.; Stillinger, F. H. Supercooled Liquids and the Glass Transition. *Nature* **2001**, *410*, 259−267.

(3) Angell, C. A.; Ngai, K. L.; McKenna, G. B.; McMillan, P. F.; Martin, S. W. Relaxation in Glassforming Liquids and Amorphous Solids. *J. Appl. Phys.* **2000**, *88*, 3113−3157.

(4) Stillinger, F. H.; Debenedetti, P. G. Glass Transition Thermodynamics and Kinetics. *Annu. Rev. Condens. Matter Phys.* **2013**, *4*, 263−285.

(5) Bretonnet, J.-L. Glass-Forming Liquids. *Mol. Phys.* **2016**, *114*, 2868−2893.

(6) Kiebel, M.; Bartsch, E.; Debus, O.; Fujara, F.; Petry, W.; Sillescu, H. Secondary Relaxation in the Glass-Transition Regime of Ortho-Terphenyl Observed by Incoherent Neutron Scattering. *Phys. Rev. B* **1992**, *45*, 10301−10305.

(7) Schnauss, W.; Fujara, F.; Sillescu, H. The Molecular Dynamics around the Glass Transition and in the Glassy State of Molecular Organic Systems: A 2 H−Nuclear Magnetic Resonance Study. *J. Chem. Phys.* **1992**, *97*, 1378−1389.

(8) Steffen, W.; Patkowski, A.; Gläser, H.; Meier, G.; Fischer, E. W. Depolarized-Light-Scattering Study of Orthoterphenyl and Comparison with the Mode-Coupling Model. *Phys. Rev. E* **1994**, *49*, 2992−3002.

(9) Cummins, H. Z.; Li, G.; Du, W.; Hwang, Y. H.; Shen, G. Q. Light Scattering Spectroscopy of Orthoterphenyl: Idealized and Extended Mode Coupling Analysis. *Prog. Theor. Phys. Suppl.* **1997**, *126*, 21−34.

(10) Monaco, G.; Fioretto, D.; Masciovecchio, C.; Ruocco, G.; Sette, F. Fast Relaxational Dynamics in the o-Terphenyl Glass. *Phys. Rev. Lett.* **1999**, *82*, 1776−1779.

(11) Petzold, N.; Rössler, E. A. Light Scattering Study on the Glass Former o-Terphenyl. *J. Chem. Phys.* **2010**, *133*, No. 124512.

(12) Kudchadkar, S. R.; Wiest, J. M. Molecular Dynamics Simulations of the Glass Former Ortho-Terphenyl. *J. Chem. Phys.* **1995**, *103*, 8566−8576.

(13) Mossa, S.; Ruocco, G.; Sampoli, M. Molecular Dynamics Simulation of the Fragile Glass Former Orthoterphenyl: A Flexible Molecule Model. II. Collective Dynamics. *Phys. Rev. E* **2001**, *64*, No. 021511.

(14) Steffen, W.; Meier, G.; Patkowski, A.; Fischer, E. W. Depolarized Light Scattering Spectroscopic Study of OTP Dynamics above Tp: A Mode Coupling Analysis Approach. *Physica A* **1993**, *201*, 300−304.

(15) Götze, W.; Sjögren, L. The Mode Coupling Theory of Structural Relaxations. *Transp. Theory Stat. Phys.* **1995**, *24*, 801−853.

(16) Götze, W.; Sjögren, L. Relaxation Processes in Supercooled Liquids. *Rep. Prog. Phys.* **1992**, *55*, 241−376.

(17) Novikov, V. N. Phonon-Density Fluctuations and Fast Relaxation in Glasses. *Phys. Rev. B* **1997**, *55*, R14685−R14688.

(18) Monaco, G.; Caponi, S.; Di Leonardo, R.; Fioretto, D.; Ruocco, G. Intramolecular Origin of the Fast Relaxations Observed in the Brillouin Light Scattering Spectra of Molecular Glass Formers. *Phys. Rev. E* **2000**, *62*, R7595.

(19) Mukamel, S. Multidimensional Femtosecond Correlation Spectroscopies of Electronic and Vibrational Excitations. *Annu. Rev. Phys. Chem.* **2000**, *51*, 691−729.

(20) Park, S.; Kwak, K.; Fayer, M. D. Ultrafast 2D-IR Vibrational Echo Spectroscopy: A Probe of Molecular Dynamics. *Laser Phys. Lett.* **2007**, *4*, 704−718.

DOI: 10.1021/acs.jpcb.7b08301
J. Phys. Chem. B 2017, 121, 10417−10428

(21) Bian, H.; Li, J.; Wen, X.; Zheng, J. Mode-Specific Intermolecular Vibrational Energy Transfer. I. Phenyl Selenocyanate and Deuterated Chloroform Mixture. *J. Chem. Phys.* **2010**, *132*, No. 184505.
(22) Yamada, S. A.; Bailey, H. E.; Tamimi, A.; Li, C.; Fayer, M. D. Dynamics in a Room-Temperature Ionic Liquid from the Cation Perspective: 2D IR Vibrational Echo Spectroscopy. *J. Am. Chem. Soc.* **2017**, *139*, 2408−2420.
(23) Sokolowsky, K. P.; Bailey, H. E.; Hoffman, D. J.; Andersen, H. C.; Fayer, M. D. Critical Slowing of Density Fluctuations Approaching the Isotropic−Nematic Transition in Liquid Crystals: 2D IR Measurements and Mode Coupling Theory. *J. Phys. Chem. B* **2016**, *120*, 7003−7015.
(24) Hoffman, D. J.; Sokolowsky, K. P.; Fayer, M. D. Direct Observation of Dynamic Crossover in Fragile Molecular Glass Formers with 2D IR Vibrational Echo Spectroscopy. *J. Chem. Phys.* **2017**, *146*, No. 124505.
(25) Maj, M.; Kwak, K.; Cho, M. Ultrafast Structural Fluctuations of Myoglobin-Bound Thiocyanate and Selenocyanate Ions Measured with Two-Dimensional Infrared Photon Echo Spectroscopy. *ChemPhysChem* **2015**, *16*, 3468−3476.
(26) Ramos, S.; Scott, K. J.; Horness, R. E.; Le Sueur, A. L.; Thielges, M. C. Extended Timescale 2D IR Probes of Proteins: p-Cyanoselenophenylalanine. *Phys. Chem. Chem. Phys.* **2017**, *19*, 10081−10086.
(27) Sokolowsky, K. P.; Fayer, M. D. Dynamics in the Isotropic Phase of Nematogens Using 2D IR Vibrational Echo Measurements on Natural-Abundance 13CN and Extended Lifetime Probes. *J. Phys. Chem. B* **2013**, *117*, 15060−15071.
(28) King, J. T.; Ross, M. R.; Kubarych, K. J. Ultrafast A-Like Relaxation of a Fragile Glass-Forming Liquid Measured Using Two-Dimensional Infrared Spectroscopy. *Phys. Rev. Lett.* **2012**, *108*, No. 157401.
(29) Perakis, F.; Hamm, P. Two-Dimensional Infrared Spectroscopy of Supercooled Water. *J. Phys. Chem. B* **2011**, *115*, 5289−5293.
(30) Tokmakoff, A. Orientational Correlation Functions and Polarization Selectivity for Nonlinear Spectroscopy of Isotropic Media .1. Third Order. *J. Chem. Phys.* **1996**, *105*, 1−12.
(31) Goldstein, M. Viscous Liquids and the Glass Transition: A Potential Energy Barrier Picture. *J. Chem. Phys.* **1969**, *51*, 3728−3739.
(32) Zheng, J.; Kwak, K.; Fayer, M. D. Ultrafast 2D IR Vibrational Echo Spectroscopy. *Acc. Chem. Res.* **2007**, *40*, 75−83.
(33) Wang, C. C.; Pecora, R. Time-Correlation Functions for Restricted Rotational Diffusion. *J. Chem. Phys.* **1980**, *72*, 5333.
(34) Lipari, G.; Szabo, A. Effect of Librational Motion on Fluorescence Depolarization and Nuclear Magnetic Resonance Relaxation in Macromolecules and Membranes. *Biophys. J.* **1980**, *30*, 489−506.
(35) Lipari, G.; Szabo, A. Model-Free Approach to the Interpretation of Nuclear Magnetic Resonance Relaxation in Macromolecules. 1. Theory and Range of Validity. *J. Am. Chem. Soc.* **1982**, *104*, 4546−4559.
(36) Moilanen, D. E.; Fenn, E. E.; Lin, Y.-S.; Skinner, J. L.; Bagchi, B.; Fayer, M. D. Water Inertial Reorientation: Hydrogen Bond Strength and the Angular Potential. *Proc. Nat. Acad. Sci. U.S.A.* **2008**, *105*, 5295−5300.
(37) Kwak, K.; Park, S.; Finkelstein, I. J.; Fayer, M. D. Frequency-Frequency Correlation Functions and Apodization in Two-Dimensional Infrared Vibrational Echo Spectroscopy: A New Approach. *J. Chem. Phys.* **2007**, *127*, No. 124503.
(38) Kwak, K.; Rosenfeld, D. E.; Fayer, M. D. Taking Apart the Two-Dimensional Infrared Vibrational Echo Spectra: More Information and Elimination of Distortions. *J. Chem. Phys.* **2008**, *128*, No. 204505.
(39) Kubo, R. A Stochastic Theory of Line Shape and Relaxation. In *Fluctuation, Relaxation, and Resonance in Magnetic Systems*; Ter Haar, D., Ed.; Oliver and Boyd: London, 1961.
(40) Kramer, P. L.; Giammanco, C. H.; Tamimi, A.; Hoffman, D. J.; Sokolowsky, K. P.; Fayer, M. D. Quasi-Rotating Frame: Accurate Line Shape Determination with Increased Efficiency in Noncollinear 2D Optical Spectroscopy. *J. Opt. Soc. Am. B* **2016**, *33*, 1143.
(41) Tokmakoff, A.; Fayer, M. D. Infrared Photon Echo Experiments: Exploring Vibrational Dynamics in Liquids and Glasses. *Acc. Chem. Res.* **1995**, *28*, 437−445.
(42) Bloem, R.; Garrett-Roe, S.; Strzalka, H.; Hamm, P.; Donaldson, P. Enhancing Signal Detection and Completely Eliminating Scattering Using Quasi-Phase-Cycling in 2D IR Experiments. *Opt. Express* **2010**, *18*, 27067.
(43) Rector, K. D.; Fayer, M. D. Vibrational Dephasing Mechanisms in Liquids and Glasses: Vibrational Echo Experiments. *J. Chem. Phys.* **1998**, *108*, 1794−1803.
(44) MacFarlane, R. M.; Shelby, R. M. Homogeneous Line Broadening of Optical Transitions of Ions and Molecules in Glasses. *J. Lumin.* **1987**, *36*, 179−207.
(45) Moog, R. S.; Ediger, M. D.; Boxer, S. G.; Fayer, M. D. Viscosity Dependence of the Rotational Reorientation of Rhodamine B in Mono- and Polyalcohols. Picosecond Transient Grating Experiments. *J. Phys. Chem.* **1982**, *86*, 4694−4700.
(46) Kramer, P. L.; Nishida, J.; Fayer, M. D. Separation of Experimental 2D IR Frequency-Frequency Correlation Functions into Structural and Reorientation-Induced Contributions. *J. Chem. Phys.* **2015**, *143*, No. 124505.
(47) Cang, H.; Li, J.; Andersen, H. C.; Fayer, M. D. Boson Peak in Supercooled Liquids: Time Domain Observations and Mode Coupling Theory. *J. Chem. Phys.* **2005**, *123*, No. 064508.
(48) Skinner, J. L. Vibrational Line Shapes and Spectral Diffusion in Fluids. *Mol. Phys.* **2008**, *106*, 2245−2253.
(49) Stephens, M. D.; Saven, J. G.; Skinner, J. L. Molecular Theory of Electronic Spectroscopy in Nonpolar Fluids : Ultrafast Solvation Dynamics and Absorption and Emission Line Shapes. *J. Chem. Phys.* **1997**, *106*, 2129−2144.
(50) Mossa, S.; Monaco, G.; Ruocco, G. Vibrational Origin of the Fast Relaxation Processes in Molecular Glass Formers. *Europhys. Lett.* **2002**, *60*, 92−98.
(51) Sastry, S.; Debenedetti, P. G.; Stillinger, F. H. Signatures of Distinct Dynamical Regimes in the Energy Landscape of a Glass-Forming Liquid. *Nature* **1998**, *393*, 554−557.
(52) Stillinger, F. H.; Weber, T. A. Hidden Structure in Liquids. *Phys. Rev. A* **1982**, *25*, 978−989.
(53) Malandro, D. L.; Lacks, D. J. Relationships of Shear-Induced Changes in the Potential Energy Landscape to the Mechanical Properties of Ductile Glasses. *J. Chem. Phys.* **1999**, *110*, 4593−4601.
(54) Malandro, D. L.; Lacks, D. J. Volume Dependence of Potential Energy Landscapes in Glasses. *J. Chem. Phys.* **1997**, *107*, 5804−5810.
(55) Phillips, W. A. Two-Level States in Glasses. *Rep. Prog. Phys.* **1987**, *50*, 1657−1708.
(56) Huber, D. L.; Broer, M. M.; Golding, B. Low-Temperature Optical Dephasing of Rare-Earth Ions in Glass. *Phys. Rev. Lett.* **1984**, *52*, 2281−2284.
(57) Berg, M.; Walsh, C. A.; Narasimhan, L. R.; Littau, K. A.; Fayer, M. D. Dynamics in Low Temperature Glasses: Theory and Experiments on Optical Dephasing, Spectral Diffusion, and Hydrogen Tunneling. *J. Chem. Phys.* **1988**, *88*, 1564−1587.
(58) Haus, J. W.; Kehr, K. W.; Lyklema, J. W. Diffusion in a Disordered Medium. *Phys. Rev. B* **1982**, *25*, 2905−2907.
(59) Jack, R. L.; Sollich, P. Duality Symmetries and Effective Dynamics in Disordered Hopping Models. *J. Stat. Mech.: Theory Exp.* **2009**, *2009*, No. P11011.
(60) Adam, G.; Gibbs, J. H. On the Temperature Dependence of Cooperative Relaxation Properties in Glass-Forming Liquids. *J. Chem. Phys.* **1965**, *43*, 139.
(61) Goldstein, M. Viscous Liquids and the Glass Transition. V. Sources of the Excess Specific Heat of the Liquid. *J. Chem. Phys.* **1976**, *64*, 4767.
(62) Angell, C. A.; Rao, K. J. Configurational Excitations in Condensed Matter, and the "Bond Lattice" Model for the Liquid-Glass Transition. *J. Chem. Phys.* **1972**, *57*, 470.
(63) Eyring, H. The Activated Complex in Chemical Reactions. *J. Chem. Phys.* **1935**, *3*, 107−115.

DOI: 10.1021/acs.jpcb.7b08301
J. Phys. Chem. B 2017, 121, 10417−10428